AIAA JOURNAL
Vol. 35, No. 12, December 1997

Static Collapse of Elastic Circular Arches

N. F. Knight Jr.* and W. S. Carron†
Old Dominion University, Norfolk, Virginia 23529-0247

The static collapse of elastic circular arches is considered. Parametric studies of elastic circular arches with different end conditions and different subtending angles are performed. These arches exhibit a collapse behavior. These simulations are based on an assumed-stress hybrid, two-node beam element, which is briefly described and then used to study the static collapse of elastic circular arches. The influence on the collapse mode of deformation of end conditions and arch geometry, as determined by the subtending angle, is discussed.

Introduction

ARCHES and curved beams represent common structural members in many aerospace, automotive, and civil engineering structures. These members generally are used as stiffeners of a shell-type structure and provide lateral support and stiffness to resist lateral loads. Because of their curvature, the load-carrying capacity is higher than that of flat or straight beams. However, they are also susceptible to large deflections and possible collapse or snapthrough. Predicting this type of response requires a nonlinear analysis to determine the structural collapse load, the collapse deformation, and the postcollapse structural response.

The structural responses of several elastic circular arches with asymmetric and symmetric boundary conditions are studied. The effect of the arch end conditions and the subtending angle on the elastic collapse behavior is determined and described. This paper briefly summarizes a formulation for an assumed-stress hybrid beam element that exploits the corotational approach for solving large-deflection problems. The element is implemented within the NASA Langley Research Center's structural analysis software framework COMET and directly coupled with its corotational utilities. The computational framework provided by COMET is also briefly described.

Element Formulation

The element formulation is based on an assumed-stress hybrid approach using the Hellinger–Reissner variational principle. This two-node beam element with 12 degrees of freedom uses independent finite element approximations for both the displacement and stress fields. The beam element is a one-dimensional element able to resist axial, torsional, shear, and bending loads about all axes. It is further assumed to be prismatic and to remain elastic during deformations. The strain-displacement relations account for transverse shear deformation and twist. Details of the element matrices and vectors are given by Deshpande[1] and Carron.[2]

The displacement and stress fields are approximated independently. The displacement degrees of freedom at each node include all six degrees of freedom (three translations and three rotations). It is assumed that the transverse shear strain is constant, and hence the transverse displacements can be described as quadratic functions along the element length, whereas the axial displacement and all rotations are assumed to vary only linearly. These approximations are written as

$$\{u\}_{6\times 1} = [N(\xi)]_{6\times 12}\{d_e\}_{12\times 1} \tag{1}$$

where $\{u\}$ is the displacement field vector, $[N]$ is a matrix of shape functions, and $\{d_e\}$ is the vector of element nodal degrees of freedom. These shape functions are derived to be consistent with the approach present by Allman[3] for drilling freedoms.

The stress field is derived within the natural coordinate system of the element by considering the equilibrium conditions for a differential beam segment. The element stress field is defined as beam resultant forces and moments over the cross section. The vector of six resultant forces and moments $\{\sigma^*\}$ are related to the unknown stress parameters $\{\beta\}$ by a matrix of polynomial approximations along the element $[P]$; that is,

$$\{\sigma^*\}_{6\times 1} = [P(\xi)]_{6\times 6}\{\beta\}_{6\times 1} \tag{2}$$

where $[P]$ is a matrix of polynomial approximation functions along the beam element length and ξ is the natural coordinate of the element. The present element has six unknown stress parameters that are used to describe a constant state of axial, torsional, and transverse shear stress resultants and a linear distribution of the bending moments along the beam element length. The assumed-stress field satisfies the equilibrium conditions in a variational sense through the Hellinger–Reissner principle.

The formulation of the beam is based on the following variational statement:

$$\pi = \sum_{e=1}^{N\text{ELEM}} \int_0^{L_e} \{\sigma^*\}^T[\partial]\{u\}\,\mathrm{d}x - \frac{1}{2}\int_0^{L_e} \{\sigma^*\}^T[C^*]^{-1}\{\sigma^*\}\,\mathrm{d}x - \int_0^{L_e} \{u\}^T\{\bar{T}\}\,\mathrm{d}x - \sum_{I=0}^{N\text{CONC}} u|_{x_I} F|_{x_I} \tag{3}$$

where the finite element approximations are made for $\{u\}$ and $\{\sigma^*\}$, $[\partial]$ represents a matrix of differential operators that relate the displacement field to the strain components, and $[C^*]$ is the constitutive matrix. The last term in Eq. (3) involves the work done by concentrated point forces and/or moments acting at x_I, and I ranges from 0 to NCONC. Substituting these approximations into the functional and then imposing the stationary conditions with respect to the nodal displacement degrees of freedom and the unknown stress parameters yields the linear stress analysis equations

$$[k_e]\{d_e\} = \{r_e\} \tag{4}$$

where $[k_e]$ is the element linear stiffness matrix, $\{d_e\}$ is the vector of element nodal displacement degrees of freedom, and $\{r_e\}$ is the vector of element work-equivalent nodal loads. The element linear stiffness matrix is computed from

$$[k_e] = [T]^T[H]^{-1}[T] \tag{5}$$

and

$$[H] = \int_0^{L_e} [P]^T[C^*]^{-1}[P]\,\mathrm{d}x \tag{6}$$

$$[T] = \int_0^{L_e} [P]^T[\partial][N]\,\mathrm{d}x \tag{7}$$

where $[P]$ is a matrix of polynomial approximation functions for the stress field and $[N]$ is a matrix of shape functions for the displacement field. These element expressions are derived using the linear

Received Feb. 9, 1996; revision received Aug. 1, 1997; accepted for publication Aug. 30, 1997.

*Professor, Department of Aerospace Engineering. E-mail: knight@aero.odu.edu. Associate Fellow AIAA.

†Graduate Research Assistant, Department of Aerospace Engineering; currently Stress Engineer, Electric Boat Corp., Building 88, D5-2, 75 Eastern Point Road, Groton, CT 06340.

strain-displacement relations at the element level and are evaluated using symbolic computations. By using the nonlinear strain-displacement relations and then linearizing the equations, the geometric stiffness matrix can be derived. The element internal force vector for the low-order corotational approach is given by

$$\{f_{\text{int}}\} = [T]^T\{\beta\} \tag{8}$$

For a geometrically nonlinear problem, this internal force vector represents the local internal force that must be projected to the global system using the corotational utilities.[4]

These element equations are then assembled, boundary conditions and point loads applied, and then these global equations are solved using an incremental-iterative Newton–Raphson approach with arc-length control.

Computational Framework

To provide access to and a proving ground for new methods in computational structural mechanics, the NASA Langley Research Center developed the finite element structural analysis software framework called COMET.[5,6] This computational framework represents a modular, machine-independent, architecturally simple, software development environment that has evolved since 1984 to accelerate the introduction and transfer research technology into large-scale applications programs. The element research reported herein is made possible through the use of COMET's generic element processor (GEP) feature,[4] and the commonality of other aspects of the analysis (assembler, solver, etc.). The GEP interface to COMET provides an effective and efficient means to develop and assess element formulations and serves as a template for element developers.

The constitutive relations for elements are defined by an independent COMET processor called the generic constitutive processor (GCP).[7] Currently the GCP only handles isotropic, homogeneous beams even though anisotropic laminated plates and shells are readily modeled. The beam constitutive relations are computed based on geometry input including possible offsets of the centroidal axes and isotropic material data. The present element uses the constitutive matrix $[C^*]$ directly in the element equations

$$\{\sigma^*\}_{6\times 1} = [C^*]_{6\times 6}\{\varepsilon^*\}_{6\times 1} \tag{9}$$

where $\{\varepsilon^*\}$ are the six strain measures for the beam consistent with the six resultant forces and moments represented by $\{\sigma^*\}$. Essentially the entries of $[C^*]$ correspond to the beam stiffness coefficients such as EA, EI_{yy}, and GJ.

The geometric nonlinear response of the element is controlled by the low-order corotational formulation offered through the GEP and its corotational utilities. Within the element, the displacements are decomposed into a rigid-body component and a deformation-causing component. Representation of the rigid-body motion is accomplished through the use of the corotational formulation wherein the element reference frame corotates with the element. The deformation-causing component is treated using the small-strain assumptions and linear strain-displacement relations at the element level. This approach is referred to as the low-order corotational formulation. If the nonlinear strain-displacement relations are used at the element level, then the approach is called a high-order corotational formulation.

The solution strategy used by COMET is based on a modified Newton–Raphson algorithm, which updates the tangent stiffness matrix at the beginning of each new step or when convergence difficulties are encountered. Arc-length control is also used because these arches exhibit limit points. In COMET, the nonlinear solution strategy is implemented in a command language procedure named NL_STATIC_1 (Ref. 8). The convergence criterion used in this study to control the solution process is based on the energy norm with a tolerance of 10^{-3}.

Numerical Results

The structural stability of circular arches is described as the loss of stability or reduction in load-carrying capacity after large deformations have occurred. In a true sense, buckling does not occur; rather collapse occurs in the nonlinear response regime. For such cases, the load-deflection curve exhibits a maximum value, often called a limit point, just prior to collapse. Researchers in finite element technology often use the circular arch with a subtending angle of 215 deg and asymmetric boundary conditions as a challenging test problem. This problem is studied herein as well. In addition, a full range of subtending angles are considered for both the asymmetric and symmetric end boundary condition case. Numerical results are compared with those of DaDeppo and Schmidt.[9,10]

Table 1 Effect of refinement on collapse load

Number of elements	Normalized collapse load $\bar{P}_{\text{cr}}$	Error %
6	9.8124	9.39
8	9.7830	9.06
10	9.4418	5.26
12	9.3602	4.35
16	9.1934	2.49
20	9.1210	1.68
24	9.0603	1.01
30	9.0423	0.81
40	9.0157	0.51
Reference solution	8.97	

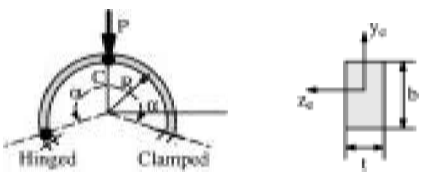

Fig. 1 Clamped-hinged circular arch: $R = 100$ in., $t = 1$ in., $b = 1$ in., $E = 12 \times 10^6$ psi, and $\nu = 0.0$.

Circular Arch Problems

The circular arches considered have the same geometry as those studied by DaDeppo and Schmidt[9] (Fig. 1). The following notation is used: P is the downward concentrated point load acting at the crown of the arch at point C, 2α is the subtending angle of the arch, R is the centroidal radius of curvature, E is the modulus of elasticity, ν is Poisson's ratio, I is the moment of inertia, U is the horizontal deflection of the crown point C, and V is the vertical deflection of the crown point C. The rectangular cross-sectional dimensions and elastic modulus are selected such that $EI = 10^6$ lb-in.^{2}. Two sets of boundary conditions are considered. One set is asymmetric and is different at the two ends of the arch (one is clamped, the other is hinged), whereas the other set is symmetric with both ends being clamped. In both cases, the applied load P at the arch crown (at point C) is normalized such that $\bar{P} = PR^2/EI$.

Common Geometry Case (2α = 215 Degrees)

The most common geometry considered by other researchers is the case for a subtending angle 2α of 215 deg and asymmetric boundary conditions.[11–15] This geometry corresponds to a deep circular arch. The solutions obtained by DaDeppo and Schmidt[9] are based on Euler's nonlinear theory of an inextensible elastica with no restrictions on the magnitude of the deflections. For this subtending angle, the normalized collapse load $\bar{P}_{\text{cr}}$ from Ref. 9 is 8.97. Numerical solutions are obtained using the present element with the low-order corotational formulation and the modified Newton–Raphson solution procedure with arc-length control.

Convergence Study

Different finite element discretizations are considered for this problem. The number of elements needed in the mesh is influenced by the nonlinear response and also by the geometry of the structure. That is, too few elements results in approximating the circular arch as a portal frame. Because the present element is a straight beam element, modeling the geometry accurately is an important driver in defining the mesh. Also, the entire arch needs to be modeled due to the asymmetry of the boundary conditions. The finite element

Table 2 Collapse load and deflection parameters for different subtending angles

2α, deg	$\bar{P}_{cr}$, reference solution[9]	$\bar{P}_{cr}$, present element	U/R, reference solution[9]	U/R, present element	V/R, reference solution[9]	V/R, present element
60	24.75	24.62	0.0113	0.0143	0.0693	0.0626
80	18.87	19.08	0.0266	0.0272	0.1260	0.1328
100	15.42	15.62	0.0515	0.0515	0.2038	0.2349
120	13.21	13.39	0.0881	0.0890	0.3061	0.3064
140	11.74	11.90	0.1384	0.1398	0.4386	0.4375
160	10.78	10.93	0.2038	0.2052	0.6074	0.6304
180	10.27	1043	0.2869	0.2904	0.8178	0.8144
190	10.23	10.39	0.3375	0.3389	0.9410	0.9504
200	10.42	10.59	0.3995	0.4035	1.0802	1.0800
205	10.71	——	0.4398	——	1.1599	——
210	11.47	11.63	0.5097	0.5072	1.2580	1.2620
210.625	11.05	——	0.5649	——	1.2228	——
211.25	10.60	——	0.5761	——	1.2013	——
212.5	9.94	——	0.5907	——	1.1739	——
215	8.97	9.12	0.6116	0.6106	1.1372	1.1310
220	7.58	7.70	0.6438	0.6466	1.0866	1.0918
230	5.72	5.81	0.6940	0.6987	1.0136	1.0238
240	4.47	4.54	0.7340	0.7299	0.9554	0.9415
260	2.86	2.91	0.7994	0.7979	0.8714	0.8659

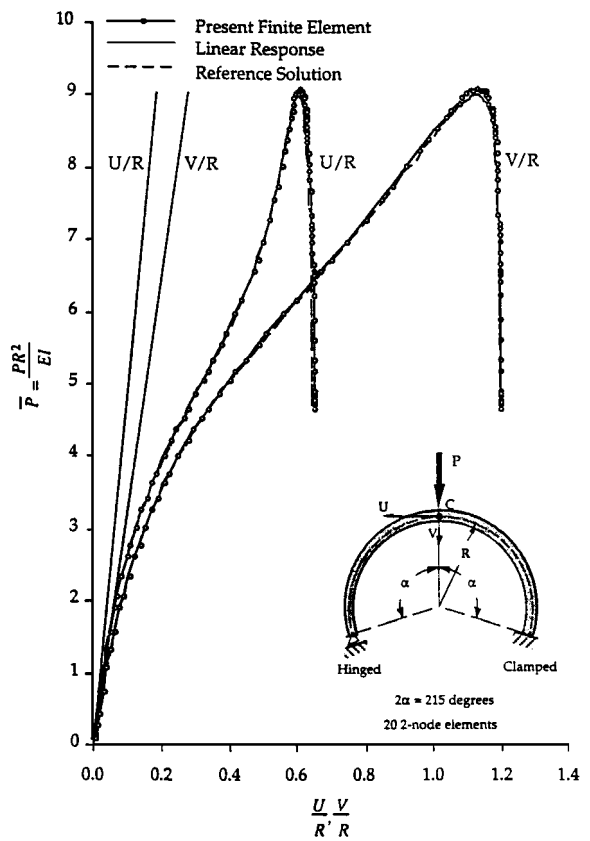

Fig. 2 Load vs deflections for clamped-hinged deep circular arch; 2α = 215 deg.

models considered herein have equal size elements with a node always at the arch crown (denoted as point C).

The normalized collapse loads obtained using various discretizations are given in Table 1 for the present element. The coarest finite element mesh considered has only six elements along the entire arch (approximately 36 deg per element) and predicts a normalized collapse load within 10% of the reference solution. With 20 elements (11 deg per element), the normalized collapse load predicted is within 1.7% of the reference solution. This level of discretization is consistent with that used by other investigators,[11–15] is representative of an accurate solution (less than a 1% change compared to the 24-element solution), and is used in all subsequent calculations.

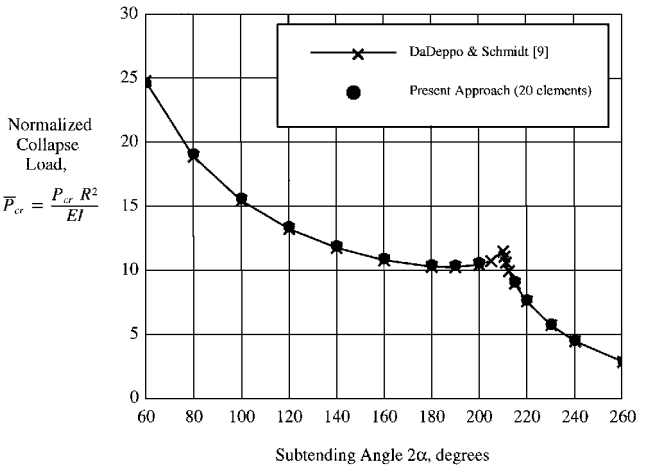

Fig. 3 Collapse load vs subtending angle for clamped-hinged circular arch.

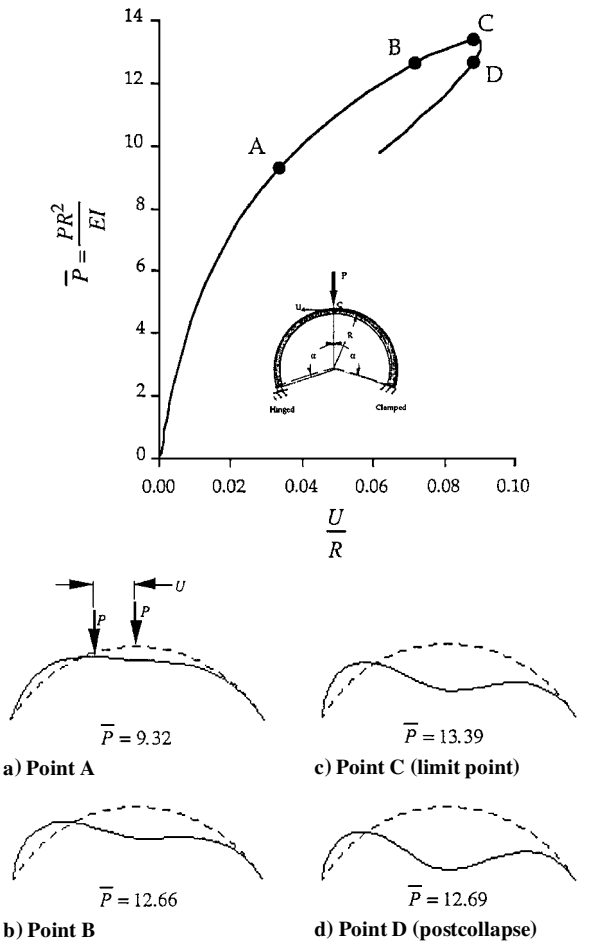

Fig. 4 Clamped-hinged circular arch with 2α = 120 deg: structural response and deformed geometries.

Nonlinear Response for 2α = 215-Degree Case

The load vs deflection curves obtained for the 20-element model are shown in Fig. 2 and compared with the analytical solutions from Ref. 9. The normalized applied load $\bar{P}$ is shown as a function of the vertical deflection V and the horizontal deflection U at point C normalized by the centroidal radius of the arch R. These results clearly indicate the accuracy of the present element and the solution approach. Also shown in Fig. 2 are the results obtained from a linear analysis, which indicate the unconservative nature of such a prediction for nonlinear softening systems.

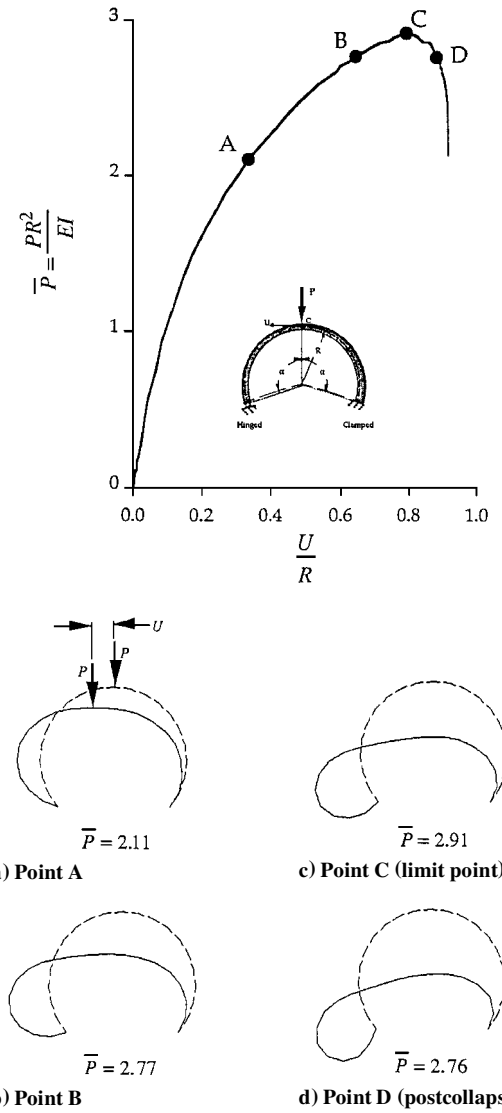

Fig. 5 Clamped-hinged circular arch with 2α = 260 deg: structural response and deformed geometries.

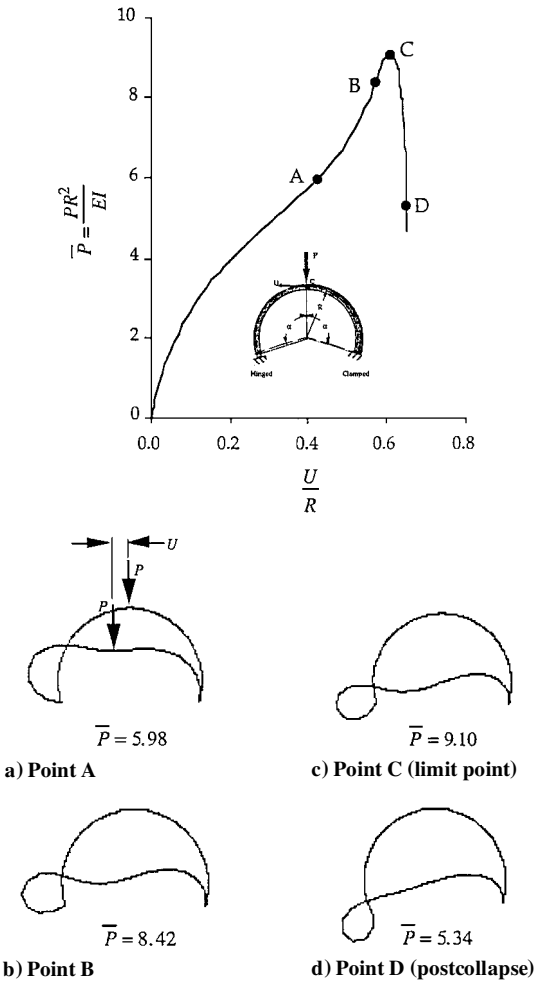

Fig. 6 Clamped-hinged circular arch with 2α = 215 deg: structural response and deformed geometries.

Effect of Subtending Angle 2α on Collapse

Using the 20-element model, the subtending angle 2α is varied to determine its effect on the structural behavior of such elastic circular arches. Results of this parametric study along with the analytical solutions obtained by DaDeppo and Schmidt[9] are presented in Table 2 and Fig. 3. The solutions obtained using the present element are in good agreement with the reference solutions. As the subtending angle increases, a cusp in the collapse load vs subtending angle curve shown in Fig. 3 occurs at approximately $2\alpha = 210$ deg. On either side of this cusp, a smooth curve appears to describe the structural behavior.

Examining the deformed geometries for arches with different subtending angles 2α on either side of the cusp reveals different structural behavior. For $2\alpha = 120$ deg, the arch exhibits a prominent local bending behavior near the arch crown, as shown in Fig. 4. The arch does not wrap around the hinged support and yet continues to snap through. For $2\alpha = 260$ deg, the arch exhibits minor local bending the near the crown, as shown in Fig. 5. However, the arch does exhibit a strong tendency to wrap around the hinged support in an asymmetric sidesway mode.

For $2\alpha = 215$ deg, the arch exhibits behavior that is more complex, as shown in Figs. 2 and 6. As the load increases from zero, the arch deforms as indicated in Fig. 6a for a load level well below the collapse load. Just prior to reaching the collapse load, the asymmetry of the arch boundary conditions, as well as a local bending response or buckle near the crown, begin to be amplified (Fig. 6b). Near the collapse load, the arch begins to wrap around the hinged support, as shown in Fig. 6c. The postcollapse behavior is shown in Fig. 6d, from which the limitations of the present 20-element discretization are apparent as large local curvatures develop near the hinged support.

By comparing the response curves given in Figs. 4–6 for these three different subtending angles, several observations can be made. First, as the value of the subtending angle increases, the slope of these load vs deflection curves prior to collapse tends to increase. Also as the angle increases, the value of the collapse load decreases except for values near the cusp in Fig. 3. Near the cusp, the load-deflection curve exhibits a rapid increase in stiffness as the collapse load is approached. For arches with a subtending angle greater than 210 deg, the nonlinear results indicate that, after very large pre-collapse deflections (when the crown has deflected vertically to the level of the supports), no further increase in the horizontal deflection U at the crown occurs. This is demonstrated by the near vertical tangent in the load vs horizontal deflection curves given in Figs. 5 and 6 after the collapse load is reached.

Effect of Boundary Conditions

Using the 20-element model, the asymmetric boundary conditions were changed so that both ends of the arch are clamped and the finite element models included the full span of the entire arch. Again, different values of the subtending angle 2α are considered to determine its effect on the structural behavior of such elastic circular arches. Results of this parametric study along with the analytical solutions obtained by DaDeppo and Schmidt[10] are presented in Fig. 7. The solutions obtained using the present element are in good agreement with the reference solutions. As the subtending angle increases, the normalized collapse load decreases in a smooth manner without any detectable cusps in the solution. For these boundary conditions, the crown of the arch deflects vertically without any horizontal deflection.

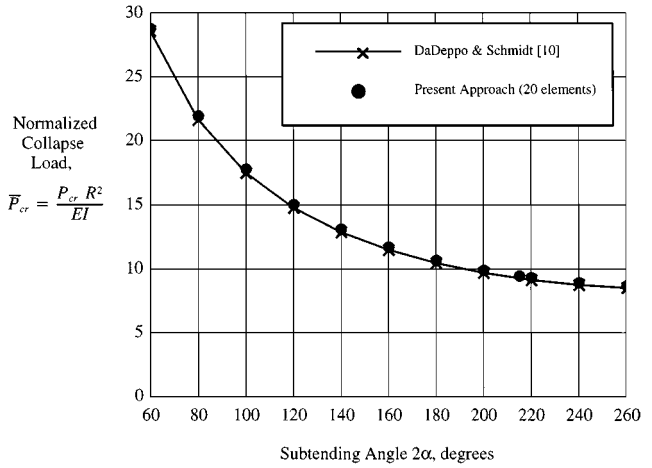

Fig. 7 Collapse load vs subtending angle for clamped-clamped circular arch.

Comparing the collapse loads as a function of subtending angle for the two sets of boundary conditions indicates that, in general, the arches with clamped ends have a higher load-carrying capacity except for subtending angles in the range near the cusp in Fig. 3. In addition, the structural behavior of the arch is also symmetric prior to collapse for the completely clamped case.

Summary

The response of elastic circular arches is studied for different end conditions and subtending angles. From the onset of loading, the response exhibits a nonlinear behavior. This behavior is often referred to as the nonlinear prebuckling response even though the behavior is that of a limit point or collapse. At the collapse load, a rapid reduction in load-carrying capacity occurs. For the case of the asymmetric end conditions, a change in the nonlinear response characteristics occurs at a subtending angle of approximately 210 deg. The response for values below this value exhibits significant local bending near the crown of the arch. The response for values above this value exhibit only minor local bending near the crown but a significant amount of wraparound near the hinge support. The response for values near 210 deg are complex combinations of both behaviors. For asymmetric boundary conditions, different structural behavior is observed for different values of the subtending angle as the load approaches the collapse value. For symmetric boundary conditions, no sidesway motion is observed.

The assumed-stress hybrid two-node beam element used in these studies has been implemented in COMET. Independent approximations are made for the displacements and stresses. The stress field is assumed to be consistent with the force and moment equilibrium equations. The displacement field is assumed to be linear along the element length except that the transverse deflections vary quadratically using the rotational degrees of freedom. The element formulation is coupled to the corotational utilities in COMET, thereby allowing the solution of large-deflection problems even though the element strain-displacementrelations only include the linear terms. The results obtained using the present element indicate its excellent performance for predicting the elastic collapse load of deep circular arches.

Acknowledgments

The research reported herein was sponsored by the NASA Langley Research Center under NASA Grant NAG-1-1505 with Alexander Tessler as the contracting officer's Technical Representative.

References

[1]Deshpande, V. S., "Development of an Assumed-Stress Hybrid C° Beam Element," M.S. Thesis, Dept. of Mechanical Engineering, Clemson Univ., Clemson, SC, Aug. 1993.

[2]Carron, W. S., "Assumed-Stress Hybrid Beam Element for Nonlinear Elastic Stress Analysis," M.S. Thesis, Dept. of Aerospace Engineering, Old Dominion Univ., Norfolk, VA, May 1995.

[3]Allman, D. J., "A Compatible Triangular Element Including Vertex Rotations for Plane Elasticity Analysis," *Computers and Structures*, Vol. 19, Nos. 1, 2, 1984, pp. 1–8.

[4]Stanley, G. M., and Nour-Omid, S., "The Computational Structural Mechanics Testbed Generic Structural Element Processor Manual," NASA CR-181728, March 1990.

[5]"The Computational Structural Mechanics Testbed Users' Manual," compiled by C. B. Stewart, NASA TM-100644 (updated), May 1990.

[6]Knight, N. F., Jr., Lotts, C. G., and Gillian, R. E., "Computational Structural Mechanics Methods Research Using an Evolving Framework," AIAA Paper 90-1145, April 1990.

[7]Hurlbut, B. J., and Stehlin, B. P., "Computational Mechanics Testbed (COMET) Generic Constitutive Processor Manual," Lockheed, CR F38484, Palo Alto, CA, May 1991.

[8]"The Computational Structural Mechanics Testbed Procedures Manual," compiled by C. B. Stewart, NASA TM-100646, Dec. 1991.

[9]DaDeppo, D. A., and Schmidt, R., "Instability of Clamped-Hinged Circular Arches Subjected to a Point Load," *Journal of Applied Mechanics*, Vol. 42, No. 4, 1975, pp. 894–896.

[10]Dadeppo, D. A., and Schmidt, R., "Large Deflection and Stability of Hingeless Circular Arches Under Interacting Loads," *Journal of Applied Mechanics*, Vol. 41, Dec. 1974, pp. 989–994.

[11]Wood, R. D., and Zienkiewicz, O. C., "Geometrically Nonlinear Finite Element Analysis of Beams, Frames, Arches, and Axisymmetric Shells," *Computers and Structures*, Vol. 7, No. 6, 1977, pp. 725–735.

[12]Pinsky, P. M., and Taylor, R. L., "A Finite Deformation Formulation for Elasto/Viscoplastic Beam Structures," *Computational Methods in Nonlinear Mechanics*, edited by J. T. Oden, North-Holland, Amsterdam, 1980, pp. 393–411.

[13]Noor, A. K., and Peters, J. M., "Penalty Finite Element Formulation for Curved Elastica," *Journal of Engineering Mechanics*, Vol. 110, No. 5, 1984, pp. 694–712.

[14]Simo, J. C., and Vu-Quoc, L., "A Three-Dimensional Finite-Strain Rod Model. Part II: Computational Aspects," *Computer Methods in Applied Mechanics and Engineering*, Vol. 58, No. 1, 1986, pp. 79–116.

[15]Sandhu, J. S., Stevens, K. A., and Davies, G. A. O., "A 3-D Co-Rotational Curved and Twisted Beam Element," *Computers and Structures*, Vol. 35, No. 1, 1990, pp. 69–79.

G. A. Kardomateas
Associate Editor